tvst

Retina

Application of 3D MRI and SS-OCT/OCTA in Assessment of Posterior Scleral Contraction for Myopic Traction Maculopathy

Danyang Yu[1,2], Di Wu[1], Haoru Li[1], Hua Rong[1], Qing He[1], Xia Zhang[1], He Xu[3], Mengdi Chai[1], Yifan Zhou[1], and Ruihua Wei[1]

[1] Tianjin Key Laboratory of Retinal Functions and Diseases, Tianjin Branch of National Clinical Research Center for Ocular Disease, Eye Institute and School of Optometry, Tianjin Medical University Eye Hospital, Tianjin, China
[2] Department of Ophthalmology, Tianjin Children's Hospital (Tianjin University Children's Hospital), Tianjin Key Laboratory of Birth Defeats for Prevention and Treatment, Tianjin, China
[3] Department of Radiology, Second Hospital of Tianjin Medical University, Tianjin, China

Correspondence: Ruihua Wei, Tianjin Key Laboratory of Retinal Functions and Diseases, Tianjin Branch of National Clinical Research Center for Ocular Disease, Eye Institute and School of Optometry, Tianjin Medical University Eye Hospital, 251 Fukang Rd., Nankai District, Tianjin 300384, China.
e-mail: rwei@tmu.edu.cn

Received: August 21, 2024
Accepted: December 18, 2024
Published: March 7, 2025

Keywords: posterior scleral contraction; myopic traction maculopathy; posterior staphyloma; 3D MRI; SS-OCT/OCTA

Citation: Yu D, Wu D, Li H, Rong H, He Q, Zhang X, Xu H, Chai M, Zhou Y, Wei R. Application of 3D MRI and SS-OCT/OCTA in assessment of posterior scleral contraction for myopic traction maculopathy. Transl Vis Sci Technol. 2025;14(3):5, https://doi.org/10.1167/tvst.14.3.5

Purpose: To evaluate the clinical efficacy and safety of posterior scleral contraction (PSC) in the treatment of myopic traction maculopathy (MTM) by three-dimensional magnetic resonance imaging (3D MRI), swept-source optical coherence tomography (SS-OCT) and swept-source optical coherence tomography angiography (SS-OCTA).

Methods: In this prospective study, 30 eyes of 25 patients with MTM were treated with PSC. The ocular parameters of the patients were measured before surgery and at 1 month, 6 months, and 1 year after 3D MRI and SS-OCT/OCTA.

Results: The differences in preoperative and postoperative parameters, including axial length (AL), spherical equivalent (SE), best-corrected visual acuity (BCVA), retinoschisis area, total posterior staphyloma height (PSH), and vitreous volume were statistically significant ($P < 0.001$). The choroidal thickness (CT) in each sector, choroidal perfusion area (CPA) in subfoveal and temporal sectors, and choroidal vascularity index (CVI) in inferior and temporal sectors increased significantly after PSC surgery ($P < 0.05$). Additionally, 3D MRI showed that the surgical strips remained strong and stable during the follow-up period, without complications such as strip displacement, fracture, and loosening.

Conclusions: The application of 3D MRI and SS-OCT/OCTA in assessment of the treatment of MTM with PSC was comprehensive with multiple ocular parameters and could further guide the clinical diagnosis and treatment of MTM.

Translational Relevance: We combined SS-OCT/OCTA and 3D MRI to provide the basis of a theory for guiding the clinical diagnosis and treatment of MTM.

Introduction

Pathologic myopia (PM) is an excessive axial length (AL) elongation associated with myopia, resulting in posterior fundus abnormalities such as posterior staphylomas, myopic maculopathy, and optic neuropathy, as well as the loss of best-corrected visual acuity (BCVA).[1] PM has become the leading cause of irreversible blindness in Asia, particularly among the working-age and elderly populations.[2–4] Studies have shown that the prevalence of PM increases with increasing spherical equivalent (SE).[5] When SE increases by 1 diopter (D), the prevalence of PM increases by 67%.[6] Myopic traction maculopathy (MTM) is a common complication

of PM, often causing hypopsia and metamorphopsia in PM patients. The different stages of MTM include myopic foveoschisis, lamellar macular hole, full-thickness macular hole, and retinal detachment.[7] The formation mechanism of MTM is bidirectional traction forces acting on the retina in both forward and backward directions, due to such factors as vitreous traction or premacular membranes generating forward traction, as well as AL growth or posterior staphylomas generating posterior traction.[8] It is essential in the treatment of MTM to relieve the forward retinal traction and control the growth of AL.

Posterior scleral contraction (PSC) is the etiological treatment for MTM. Pan et al.[9] modified the traditional posterior scleral reinforcement such that the expanded posterior sclera was contracted to release the traction effect on the retina and thus promote recovery of the MTM. It can effectively shorten AL and control the growth rate of AL, giving rise to its being referred to as PSC. Some common examination methods used to assess the effect of PSC have their own advantages. Swept-source optical coherence tomography (SS-OCT) can clearly and directly observe the retinal structure. Three-dimensional magnetic resonance imaging (3D MRI) can observe the morphology of posterior staphylomas and the location of surgical strip, as well as measure the vitreous volume, which can reflect the contraction of the strip objectively and spatially.[10] As a new noninvasive and quantitative method to visualize choroidal microvasculature, swept-source optical coherence tomography angiography (SS-OCTA) has been used to observe the changes of choroidal thickness and choroidal blood flow in PM patients.[11] Using a single examination method has its limitations with regard to evaluating surgical effects. SS-OCT can well observe the structure of each layer of retina and measure the posterior staphyloma height (PSH), but it cannot observe the complete morphology of posterior staphylomas. 3D MRI can completely observe the shape of the eyeball and the location of the surgical strip, but it cannot reveal each layer of retina and choroid. SS-OCTA can quantify choroidal blood flow and evaluate the effect of surgical strips on fundus blood supply, but it cannot directly observe surgical strips and quantify changes in retinal structure. Thus, combined application of SS-OCT, SS-OCTA, 3D MRI, and other ophthalmic examinations can provide a more comprehensive assessment.

In this study, 3D MRI and SS-OCT/OCTA was applied to evaluate the effect of PSC on various aspects of visual function, retinal structure, and choroidal blood perfusion. We quantified the imaging results to more comprehensively and accurately observe the recovery of MTM, which can further guide clinical diagnosis and treatment.

Methods

Subjects

This prospective study was conducted at Tianjin Medical University Eye Hospital and included 30 eyes from 25 patients with MTM who were treated by PSC. The initial inclusion criteria were age > 18 years, SE ≤ −6.00 D, and AL ≥ 26 mm with MTM. All subjects were excluded from this study who had a history of ocular trauma, severe cataract, choroidal or other eye diseases, related systemic diseases, claustrophobia, or metal implants that could interfere with the surgery and ophthalmic examinations. The study adhered to the tenets of the Declaration of Helsinki and was approved by the Ethics Committee of Tianjin Medical University Eye Hospital (2022KY(L)-34). The potential benefits and risks of PSC were thoroughly discussed with all patients included in this study, and they all provided written informed consent.

Ophthalmic Examinations

All patients with MTM were evaluated at preoperative, 1-month, 6-month, and 1-year follow-up visits. The preoperative and postoperative examinations included slit-lamp biomicroscopy, BCVA, SE (KR-800 Auto Kerato-Refractometer; Topcon Healthcare, Tokyo, Japan), AL (Lenstar LS900; Haag-Streit, Köniz, Switzerland), intraocular pressure (IOP; CT-1 Computerized Tonometer; Topcon Healthcare), SS-OCT/OCTA (VG200S; SVision Imaging, Henan, China), and 3D MRI (GE Healthcare, Chicago, IL).

We used SS-OCT, SS-OCTA, and 3D MRI to evaluate the changes of fundus structure at the same position at different time points before and after surgery in order to continuously observe the recovery of MTM over time. From the retinal structure level, SS-OCT was used to compare retinoschisis area and PSH to show reattachment of the retina and the size of posterior staphylomas. From the structure of the eyeball, 3D MRI was used to compare vitreous volume to reflect the changes in the size of posterior staphylomas and contraction of the surgical strips. With regard to fundus blood supply, SS-OCTA was used to compare choroidal thickness (CT), choroidal perfusion area (CPA), choriocapillaris perfusion area (CCPA), and choroidal vascularity index (CVI) to observe the effect of surgical strips on choroid and its blood flow.

SS-OCT/OCTA Image Acquisition

The VG200S SS-OCT/OCTA system was equipped with an advanced swept-source system that includes an

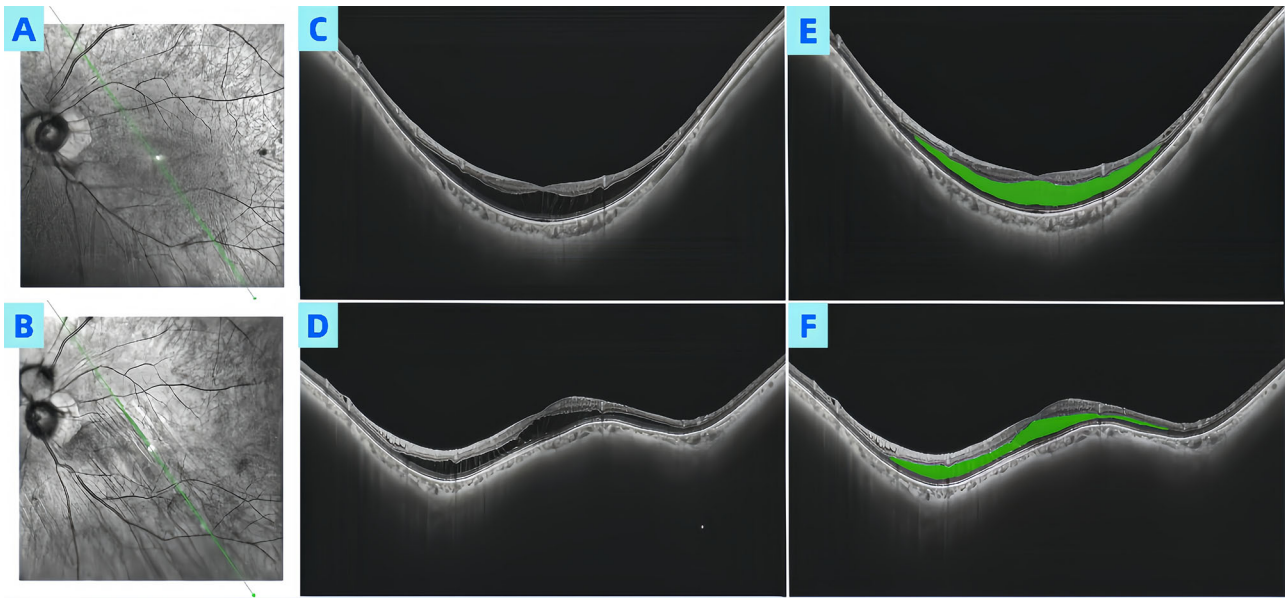

Figure 1. The preoperative and postoperative retinoschisis area. (**A**–**B**) showed the same scan line before and after surgery by SS-OCT. (**C**–**D**) showed the OCT images with the largest retinoschisis area before and after surgery. (**E**–**F**) showed that the retinoschisis area (*green*) was measured automatically by the SS-OCT proprietary measuring tool, excluding the area of local retinal detachment.

eye-tracking program based on an integrated confocal scanning laser funduscope, which was very good at removing motion artifacts.[12] SS-OCT was performed with 36 radial scan lines centered on the fovea, and each measurement produced 36 images. We selected the most obvious retinoschisis in the 36 preoperative OCT images to measure the largest retinoschisis area and used this scanning direction as the standard for each measurement after surgery. We manually identified the edge of the retinoschisis and automatically calculated the retinoschisis area by SS-OCT (Fig. 1). We selected two images (superior and inferior direction, nasal and temporal direction) from 36 OCT images to measure PSH. Each PSH was measured as the vertical distance between the subfoveal retinal pigment epithelium (RPE) and the peripheral RPE 3 mm from the fovea in the superior, inferior, nasal, and temporal directions (Fig. 2). The sum of these four heights was the total PSH, which is used to represent PSH in this study. The SS-OCT parameters were measured three times manually and averaged by an experienced ophthalmologist.

SS-OCTA images were obtained with a raster scan protocol of 512 × 512 B-scans, which covered an area of 6 × 6 mm centered on the fovea. According to the Early Treatment Diabetic Retinopathy Study (ETDRS) grid, the macular region was divided into three concentric rings with diameters of 1 mm (central fovea [C]), 3 mm (parafovea), and 6 mm (perifovea). The parafoveal region was divided into four regions: superior (S), inferior (I), nasal (N), and temporal (T) (Fig. 3). In order to ensure the accuracy of the results, only foveal and parafoveal regions (including C, S, I, N, and T) were used for analysis. The microcirculation parameters of the choroidal layer included CT, CPA, CCPA, and CVI at subfoveal, superior, inferior, nasal, and temporal sectors (Fig. 4). CT was defined as the vertical distance between the outer edge of RPE and the outer edge of the choroid. The choriocapillaris was automatically defined by the system as the microvasculature from the basal border of the RPE-Bruch's membrane complex to 20 µm below it.[12] All measurements of the choroidal microcirculation parameters were automatically calculated and derived by SS-OCTA, supervised and verified by an experienced ophthalmologist. In this study, some patients were older with severe MTM and the choriocapillaris was so thin that we manually stratified to ensure the authenticity of data export.

Three-Dimensional MRI

For the 3D MRI examination in this study, a Discovery MR750 3.0T scanner (GE Healthcare) with eight-channel phased-array head coils was used. Axial images were acquired using a fast-recovery fast spin-echo acceleration sequence (3D FRFSE-XL) with high image quality using the following imaging parameters: repetition time of 8000 ms, echo time of 800 ms, field of view of 18 mm^2 × 18 mm^2, matrix size of 256 × 256, echo train length of 70, band width of 62.5 Hz, slice thickness of 1 mm, and flip angle of 90°. The total scan time for each subject was 8 minutes, 41 seconds, and the number of acquired layers was 112. The images presented in this sequence show that

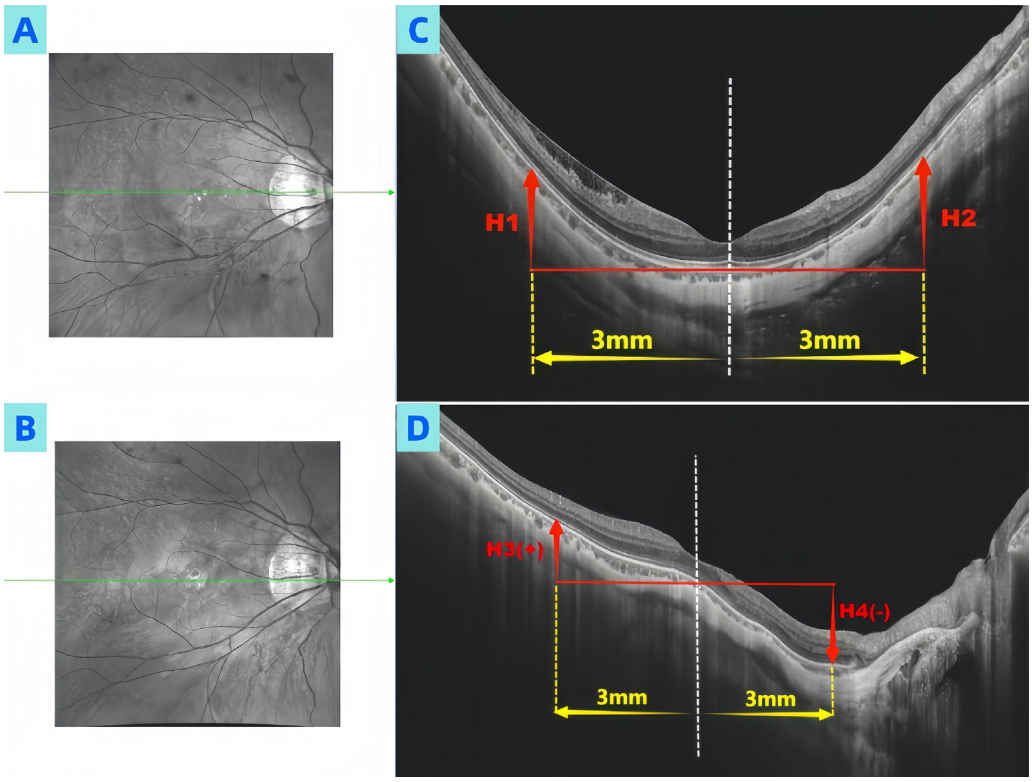

Figure 2. Typical OCT images of the same patient before and after surgery. (**A**–**B**) showed the same scan line before and after surgery by SS-OCT. (**C**) A point 3 mm from the fovea was identified on both sides at which the PSH was measured (H1 and H2), defined as the vertical distance between the subfoveal retinal pigment epithelium line and that on either side. (**D**) The PSH was expressed as a positive number (H3) if the edge was located anteriorly and a negative number (H4) if it was posterior.

tissues with higher water content are high signal, as the vitreous body has a high water content and is shown to be highly luminous on the image relative to its surrounding tissues. We performed 3D MRI examination for the patient before surgery and at 1 month, 6 months, and 1 year after surgery and obtained the source files. We utilized Python software to process and analyze the MRI Digital Imaging and Communications in Medicine (DICOM) files to calculate the vitreous volume. Through the change of vitreous volume, we can know the contraction strength of the surgical strips on the posterior scleral.

PSC Surgery Procedure

All surgeries were performed microscopically by the same experienced surgeon. The strips used for surgery were allogeneic endocranium, which was cross-linked by 0.1% genipin. After induction of general anesthesia, the pruned strip was put on the posterior pole of the eye. The nasal end of the strip was fixed to the equatorial anterior sclera between the inferior and internal rectus muscles, and the temporal end was fixed to the equatorial sclera between the superior and external rectus muscles. Before fixation, the anterior chamber was punctured with a needle, and two to four drops of atrial fluid were released to balance the IOP. Surgical details were described in our previous paper.[13]

Statistical Analysis

Statistical analysis was performed using SPSS Statistics 26.0 (IBM, Chicago, IL). Descriptions of the quantitative data are presented as the mean ± SD. Repeated-measures analysis of variance (RMANOVA) with the post hoc least significant difference (LSD) test was used to assess the differences between before surgery and 1 month, 6 months, and 1 year after PSC. $P < 0.05$ indicates a statistically significant difference.

Results

The participants included five males and 20 females, with a mean age of 52.36 ± 12.69 years, and they were followed up for 1 year. The postoperative changes in BCVA, SE, AL, IOP, retinoschisis area, and vitreous volume are shown in Table 1. The differences between preoperative and postoperative BCVA, SE,

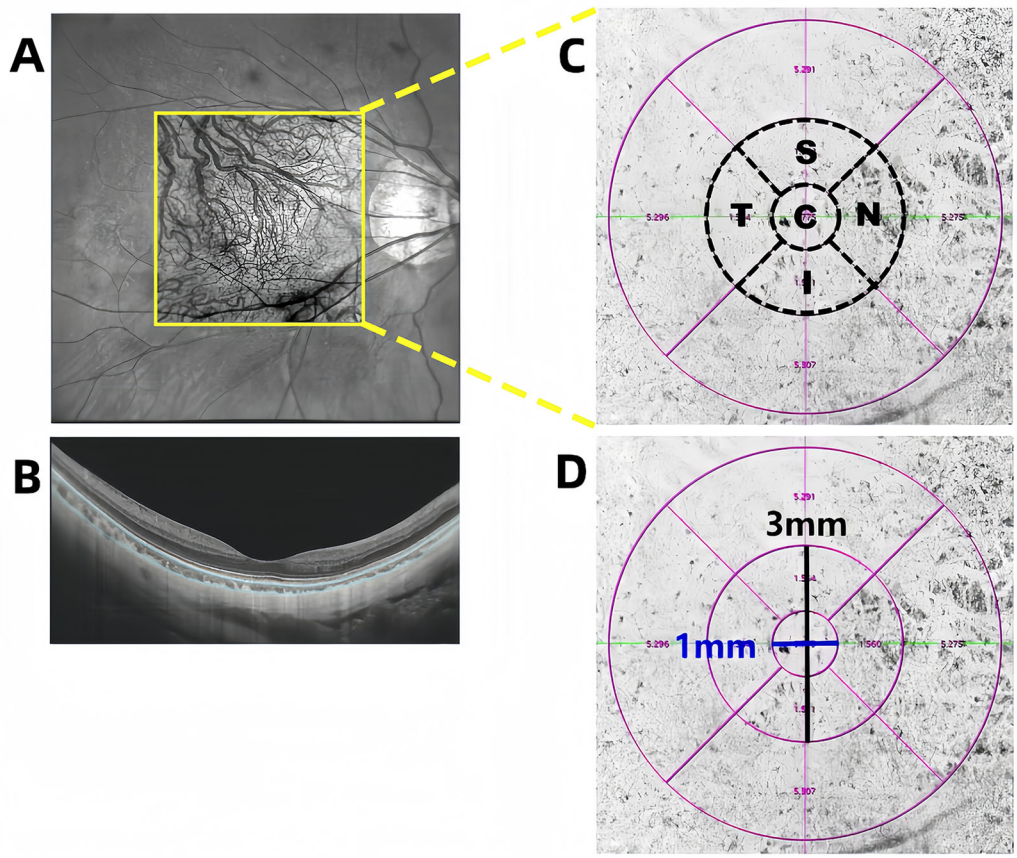

Figure 3. Illustration of choroidal blood perfusion analysis. (**A**) OCTA scan region of 6 × 6 mm. (**B**) OCT image with choroidal layer segmentation lines. (**C**–**D**) Magnified en face OCTA choroidal image with ETDRS grid. The foveal region (**C**) was a 1-mm-diameter circle centered on the fovea. The parafoveal region was a 1- to 3-mm-diameter ring, divided into four regions: superior (S), inferior (I), nasal (N) and temporal (T).

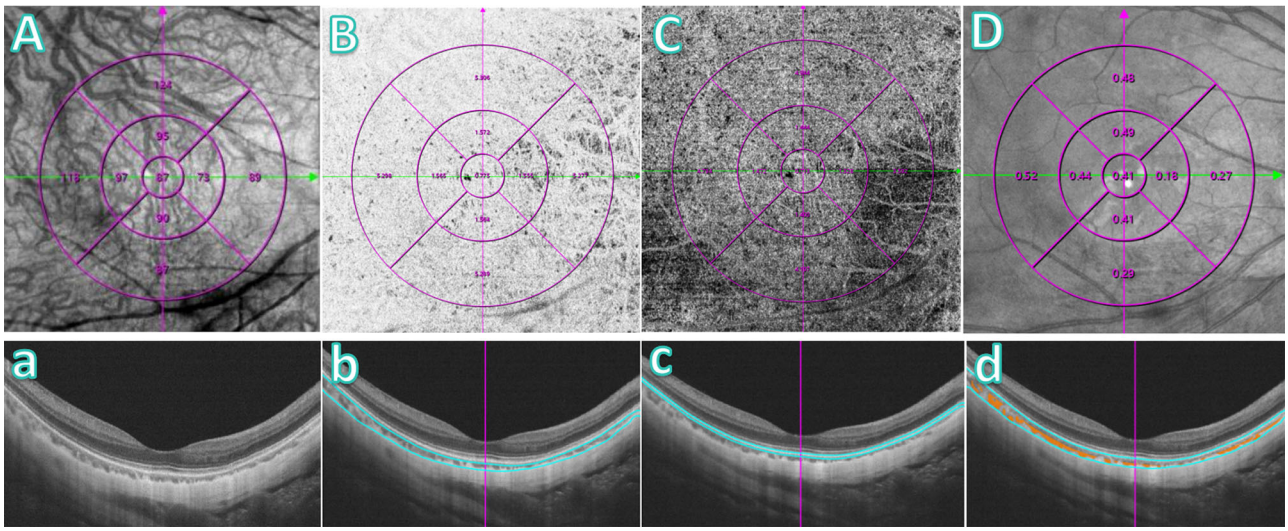

Figure 4. The CT, CPA, CCPA, and CVI were measured by SS-OCTA, based on the ETDRS contour. (**A**–**D**) The en face OCTA images of CT, CPA, CCPA and CVI. (**a**) B-scans image without annotation. (**b**) B-scans image with segmentation lines of CT and CPA. (**c**) B-scans image with segmentation lines of CCPA. (**d**) B-scans image with segmentation lines of CVI.

Table 1. Results of Preoperative and Postoperative Examinations (Mean ± SD)

Parameter	Baseline	1 Month	6 Months	12 Months	*P*[a]
BCVA (logMAR)	0.69 ± 0.59	0.69 ± 0.53	0.60 ± 0.59[b]	0.50 ± 0.50[b]	**<0.001**
SE (D)	−15.69 ± 5.66	−11.20 ± 5.50[b]	−11.69 ± 5.48[b]	−11.97 ± 5.46[b]	**<0.001**
AL (mm)	30.58 ± 2.05	28.45 ± 2.34[b]	28.87 ± 2.24[b]	29.00 ± 2.25[b]	**<0.001**
Retinoschisis area (mm^2)	1.31 ± 1.24	0.51 ± 0.51[b]	0.24 ± 0.40[b]	0.10 ± 0.18[b]	**<0.001**
Vitreous volume (mm^3)	7770.17 ± 1494.46	7101.06 ± 1406.42[b]	7359.24 ± 1445.62[b]	7443.45 ± 1459.45[b]	**<0.001**
IOP (mm Hg)	14.85 ± 2.58	13.53 ± 3.20[b]	14.44 ± 2.49	14.43 ± 2.96	**0.055**

Boldface entries indicate *P* values < 0.05.
[a]Based on RMANOVA.
[b]$P < 0.05$ by multiple comparisons (LSD post hoc test) versus the baseline.

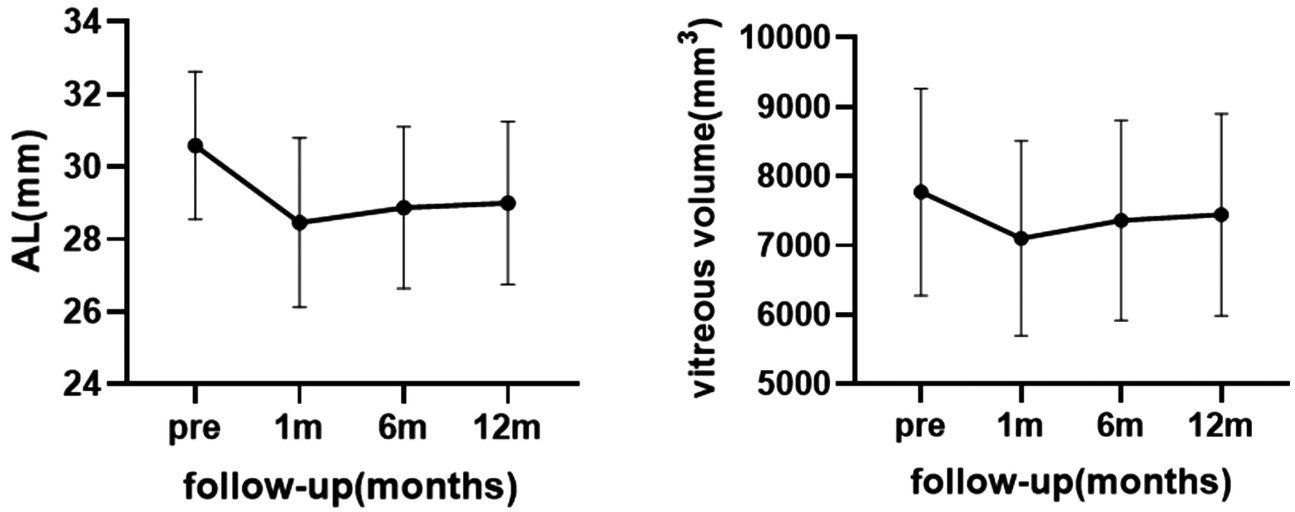

Figure 5. Changes in AL and vitreous volume after PSC.

AL, retinoschisis area, and vitreous volume were statistically significant ($P < 0.001$). There was no significant difference in IOP changes. The changes of AL and vitreous volume shown in Figure 5 indicate that the AL and vitreous volume were decreased after the surgery, but there was an increase during the 6 months after PSC which remained stable after 6 months. The retinoschisis area decreased after PSC; even the retinoschisis of 21 eyes (70%) disappeared. The postoperative BCVA was significantly higher than

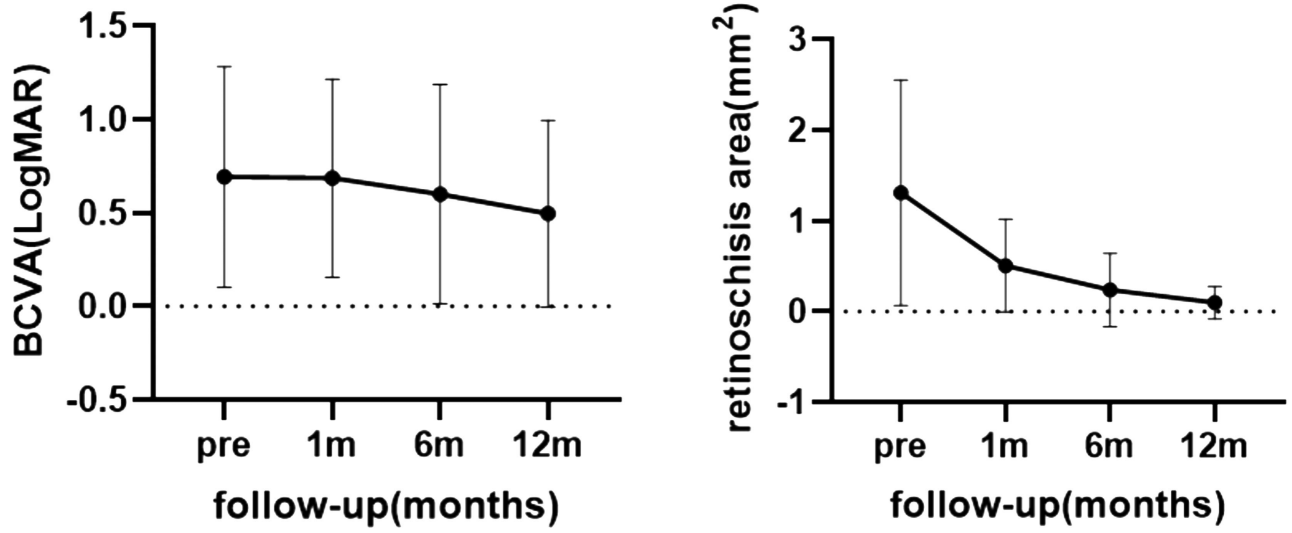

Figure 6. Changes in BCVA and retinoschisis area after PSC.

Table 2. Preoperative and Postoperative Measurements of PSH of Superior, Inferior, Nasal, and Temporal Subfields

Parameter	Baseline	1 Month	6 Months	12 Months	P[a]
PSH superior (μm)	513.03 ± 409.94	−343.85 ± 545.27[b]	−284.60 ± 442.82[b]	−366.41 ± 464.46[b]	**<0.001**
PSH inferior (μm)	264.62 ± 286.71	550.79 ± 486.82[b]	512.33 ± 524.34[b]	536.03 ± 410.33[b]	0.074
PSH nasal (μm)	280.99 ± 390.84	−708.73 ± 701.23[b]	−574.87 ± 575.34[b]	−566.11 ± 452.22[b]	**<0.001**
PSH temporal (μm)	492.58 ± 314.35	761.72 ± 640.04	766.83 ± 538.69[b]	709.65 ± 513.76	0.106
Sum of PSH (μm)	1551.23 ± 823.56	259.93 ± 1100.92[b]	493.18 ± 1010.80[b]	313.16 ± 915.45[b]	**<0.001**

Boldface entries indicate P values < 0.05.
[a]Based on RMANOVA.
[b]$P < 0.05$ by multiple comparisons (LSD post hoc test) versus the baseline.

Table 3. Preoperative and Postoperative Measurements of CT, CPA, CCPA, and CVI

Parameter	Baseline	1 Month	6 Months	12 Months	P[a]
CT subfoveal (μm)	86.86 ± 40.04	137.83 ± 43.15[b]	119.06 ± 42.49[b]	114.86 ± 37.66[b]	**<0.001**
CT superior (μm)	98.69 ± 39.83	135.74 ± 46.37[b]	118.20 ± 41.18[b]	115.03 ± 39.93[b]	**<0.001**
CT inferior (μm)	90.97 ± 38.06	133.54 ± 37.17[b]	110.85 ± 31.29[b]	112.47 ± 31.49[b]	**<0.001**
CT nasal (μm)	87.72 ± 36.13	128.00 ± 41.70[b]	110.26 ± 42.31[b]	110.08 ± 38.79[b]	**<0.001**
CT temporal (μm)	91.69 ± 41.08	137.14 ± 38.36[b]	112.77 ± 37.69[b]	111.82 ± 38.34[b]	**<0.001**
CPA subfoveal (mm^2)	0.76 ± 0.04	0.77 ± 0.02[b]	0.77 ± 0.03	0.76 ± 0.03	**0.043**
CPA superior (mm^2)	1.50 ± 0.13	1.52 ± 0.12	1.51 ± 0.11	1.51 ± 0.11	0.439
CPA inferior (mm^2)	1.50 ± 0.13	1.54 ± 0.13[b]	1.52 ± 0.14	1.52 ± 0.15	0.136
CPA nasal (mm^2)	1.50 ± 0.13	1.51 ± 0.14	1.50 ± 0.15	1.50 ± 0.15	0.377
CPA temporal (mm^2)	1.49 ± 0.15	1.52 ± 0.16	1.52 ± 0.16	1.51 ± 0.17	**0.002**
CCPA subfoveal (mm^2)	0.57 ± 0.11	0.60 ± 0.08	0.59 ± 0.07	0.59 ± 0.09	0.057
CCPA superior (mm^2)	1.04 ± 0.33	1.09 ± 0.28	1.09 ± 0.25	1.09 ± 0.25	0.836
CCPA inferior (mm^2)	1.08 ± 0.23	1.14 ± 0.25	1.14 ± 0.23	1.12 ± 0.23	0.187
CCPA nasal (mm^2)	0.99 ± 0.28	1.04 ± 0.27	1.02 ± 0.29	1.03 ± 0.30	0.472
CCPA temporal (mm^2)	0.95 ± 0.31	1.04 ± 0.28[b]	1.04 ± 0.26[b]	1.02 ± 0.25	0.128
CVI subfoveal (%)	0.21 ± 0.18	0.27 ± 0.15	0.21 ± 0.12	0.19 ± 0.13	0.081
CVI superior (%)	0.26 ± 0.15	0.30 ± 0.11	0.26 ± 0.12	0.26 ± 0.13	0.130
CVI inferior (%)	0.21 ± 0.15	0.29 ± 0.13[b]	0.22 ± 0.11	0.22 ± 0.11	**0.007**
CVI nasal (%)	0.26 ± 0.15	0.27 ± 0.13	0.22 ± 0.14	0.22 ± 0.12	0.091
CVI temporal (%)	0.27 ± 0.17	0.33 ± 0.12	0.26 ± 0.10	0.26 ± 0.11	**0.002**

Boldface entries indicate P values < 0.05.
[a]Based on RMANOVA.
[b]$P < 0.05$ by multiple comparisons (LSD post hoc test) versus the baseline.

the preoperative level, and the visual function was improved (Fig. 6).

Compared with the preoperative data, the total PSH after PSC was obviously decreased and statistically significant ($P < 0.001$). PSH of superior and nasal subfields decreased and fell to negative values postoperatively, with a statistically significant difference over time ($P < 0.001$). PSH of inferior and temporal subfields increased postoperatively with no statistically significant difference in change over time ($P > 0.05$) (Table 2).

Postoperative results of CT, CPA, CCPA, and CVI are presented in Table 3. The CT of the central subfield and parafoveal subfields increased significantly after PSC surgery during follow-up ($P < 0.001$). The subfoveal and temporal CPA increased significantly after PSC surgery ($P < 0.05$), and the inferior and temporal CVI were increased after PSC surgery ($P < 0.05$). CCPA did not change significantly compared to preoperative measurements (Table 3; Fig. 7). Figure 8 shows two typical cases. SS-OCT/OCTA and 3D MRI were used to observe

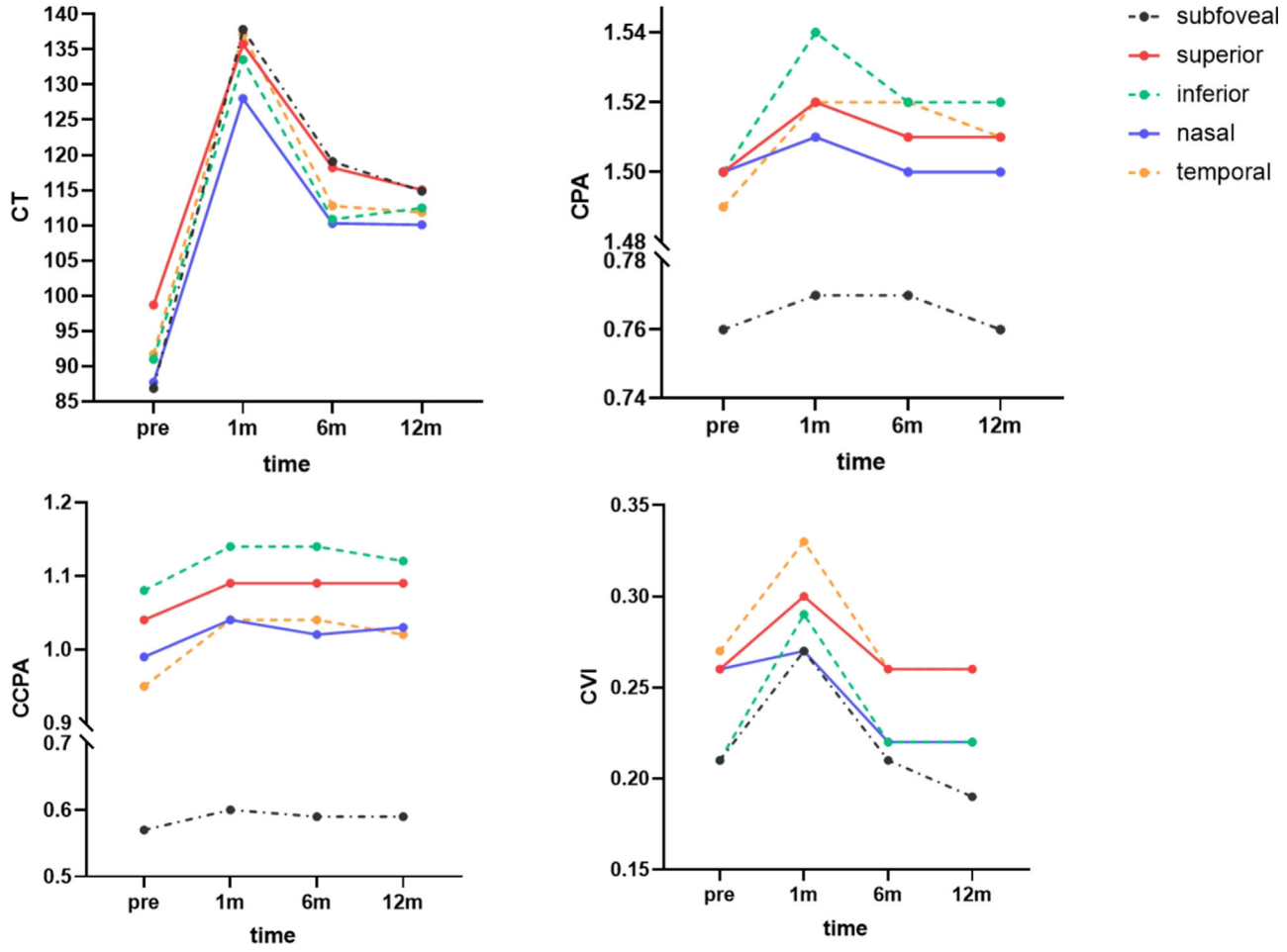

Figure 7. Preoperative and postoperative measurements of CT, CPA, CCPA, and CVI.

qualitatively that in each case the retinoschisis was attached, the posterior staphyloma was reduced, the strip positions were correct, and the microcirculatory function was normal at 1 year after PSC compared with baseline.

Discussion

In this study, we used 3D MRI and SS-OCT/OCTA) to evaluate the efficacy and safety of PSC for the treatment of MTM. PSC is an etiological treatment for PM, which can effectively shorten the AL, promote retinal anatomic reattachment, improve microcirculation of the fundus, and improve the visual function without damaging intraocular tissues. In previous studies,[14–16] researchers often used only OCT to evaluate the reattachment of retina after PSC but did not quantify the OCT images. Some researchers combined OCT and 3D MRI to observe morphology of the eyeball in PM patients and analyzed the relationship between posterior staphyloma and myopic retinoschisis, but they did not investigate its application in the long-term follow-up of PSC.[17–19] With the continuous development of imaging technology, the development of ophthalmic imaging instruments with higher resolution, wider imaging range, and greater convenience offer the potential for efficient and precise diagnosis and treatment of PM. In this study, we combined SS-OCT/OCTA and 3D MRI to provide a more reliable clinical basis for precise diagnosis and treatment of MTM.

The results of this study showed that AL was significantly shortened after PSC and remained stable at 6 months postoperatively, effectively controlling the progression of PM. We processed the information contained in the 3D MRI using Python software to calculate the vitreous volume of the eyeball, which was significantly reduced postoperatively due to the contractile effect of the surgical strip, and the trend of change was essentially the same as that of AL.

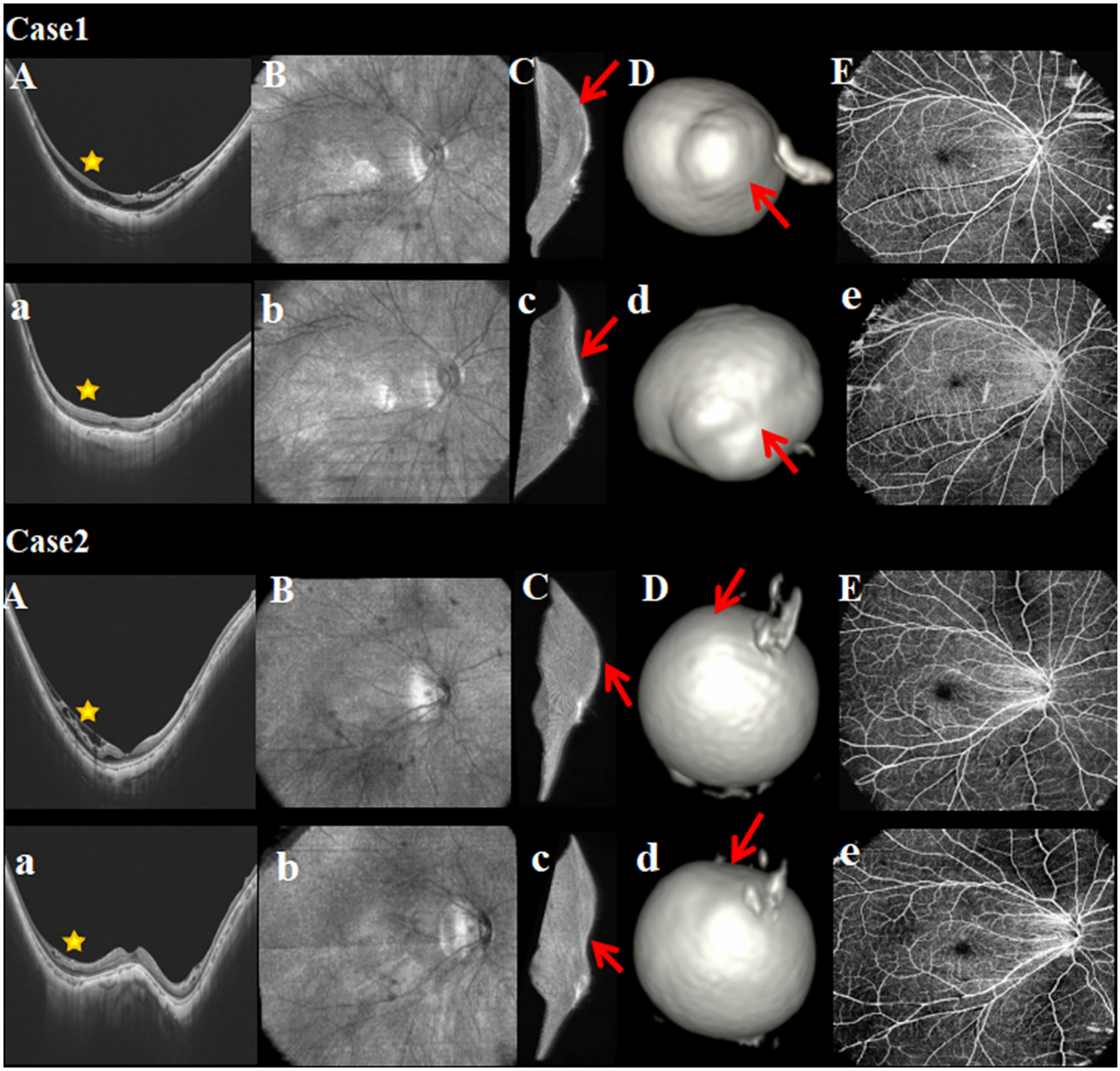

Figure 8. Preoperative and postoperative SS-OCT/OCTA and 3D MRI images of two typical cases. (**A**–**E**) Images before PSC. (**a**–**e**) Images at 1 year after PSC. The *yellow stars* indicate changes in retinoschisis, and the *red arrows* indicate changes in the posterior staphyloma.

In this study, we used the measurement tool of SS-OCT to measure the area of retinoschisis before and after surgery. The results show that retinoschisis area decreased after PSC, and the retinoschisis even disappeared in 21 eyes (70%) at the end of follow-up. Some previous studies used height to represent the size of the retinoschisis cavity.[20–22] However, the method of measuring the height to represent the whole retinoschisis cavity size has its limitations. The height cannot fully represent the recovery of MTM, and it is easily influenced by subjective factors. Toyama et al.[23] found that the degree of MTM is related to baseline vision. In our study, we found that postoperative BCVA improved and retinoschisis area decreased significantly compared with the baseline, but Toyama et al.[23] showed the opposite trend (Fig. 6). We think the BCVA improvement could be due to the gradual recovery of retinal anatomical structure and improved refractive state after PSC. But, the degree of BCVA improvement varied from person to person and may be related to the severity of MTM, as well as other influencing factors, such as retinal choroidal atrophy.

The PSH imaged by SS-OCT showed that the difference in PSH on the inferior and temporal sides was not

statistically significant; however, the difference in PSH on the superior and nasal sides showed a statistically significant decrease, suggesting that the location of the surgical strip in the macular area may have been biased towards the temporal and inferior sides. This conclusion was also corroborated by the choroidal blood flow results. Zhang et al.[24] found that both superficial and deep macular blood flow density and index increased after surgery. Zhang et al.[11] found that CT, CPA, and CCPA increased significantly at 1 week postoperatively. CVI is a newer parameter that can be used to noninvasively assess vascular status of the choroid.[25] As a more accurate and stable indicator, it has good repeatability and low variability and is not easily affected by other physiological factors.[26,27] For these reasons, we added CVI to the evaluated choroidal blood flow parameters. In our study, the CPA and CVI measured by SS-OCTA showed more pronounced increases on the inferior and temporal side. This finding may be related to the fact that the strips are located inferior and temporal to the fovea, stimulating an inflammatory response in the scleral tissue and promoting neoangiogenesis.

The differences in preoperative and postoperative IOP found in this study were not significant. In order to maintain IOP stability and prevent compression of ocular tissues by an increase in IOP due to scleral contraction, we punctured the anterior chamber during surgery and released several drops of atrial fluid, depending on the amount of contraction.

Three-dimensional MRI can show the eyeball morphology completely and stereoscopically, which is a good way to observe posterior staphylomas. 3D MRI combined with Zernike polynomials can quantitatively analyze posterior staphylomas and more fully utilize the information provided by the 3D MRI to more objectively describe the morphology of the posterior surface of the eyeball.[28] 3D MRI can show the extent of posterior staphylomas and their positional relationship with the optic nerve, which can be used to design the surgical plan.[29] Additionally, 3D MRI combined with 3D printing technology can restore the morphology of the eyeball in equal proportions, which can help doctors choose the appropriate surgical strips, avoid blood vessels and the optic nerve during surgery, reduce surgical complications, and improve the success rate of surgery.[30] In this study, we found that the surgical strips remained stable and posterior staphylomas were effectively controlled at the end of follow-up. The results of PSC can be comprehensively evaluated by SS-OCT/OCTA, and 3D MRI indicates that the use of PSC is safe and effective.

This study does have some shortcomings, such as the small sample size, a short follow-up period, and the lack of binocular contrast. Due to the sample size limitation, the types of posterior staphylomas and stages of MTM were not classified and discussed. And the choroidal and choriocapillaris perfusion analysis were acquired directly from the OCT machine, which will require a more careful validation by expanding the sample size in the future, so as to provide richer clinical information for assessing the long-term efficacy and safety of PSC.

Conclusions

3D MRI and SS-OCT/OCTA could be used to evaluate various aspects of surgical PSC and comprehensively and accurately observe the recovery of MTM, which could further guide clinical diagnosis and treatment.

Acknowledgments

The authors thank all of the members of our study. Additionally, we appreciate the generous support offered by the Tianjin Key Laboratory of Retinal Functions and Diseases, Tianjin Branch of National Clinical Research Center for Ocular Disease, Eye Institute and School of Optometry, Tianjin Medical University Eye Hospital, for this study.

Supported by Tianjin Key Medical Discipline (Specialty) Construction Project (TJYXZDXK-037A). The funding organization had no role in the design or conduct of this research.

Author Contributions: All authors contributed to the study conception and design. DY, DW, HL, HR, QH, XZ, HX, MC and YZ collected the data. DY analyzed the data and wrote the manuscript. RW verified the analytical methods, provided critical feedback, and helped revise the final manuscript. All authors read and approved the final manuscript.

Disclosure: **D. Yu**, None; **D. Wu**, None; **H. Li**, None; **H. Rong**, None; **Q. He**, None; **X. Zhang**, None; **H. Xu**, None; **M. Chai**, None; **Y. Zhou**, None; **R. Wei**, None

References

1. Ohno-Matsui K, Wu P-C, Yamashiro K, et al. IMI pathologic myopia. *Invest Ophthalmol Vis Sci*. 2021;62:5.

2. Xu L, Wang Y, Li Y, et al. Causes of blindness and visual impairment in urban and rural areas in Beijing: the Beijing eye study. *Ophthalmology*. 2006;113:1134.e1–e11.
3. Hsu WM, Cheng CY, Liu JH, Tsai SY, Chou P. Prevalence and causes of visual impairment in an elderly Chinese population in Taiwan: the Shihpai eye study. *Ophthalmology*. 2004;111:62–69.
4. Iwase A, Araie M, Tomidokoro A, Yamamoto T, Shimizu H, Kitazawa Y. Prevalence and causes of low vision and blindness in a Japanese adult population: the Tajimi study. *Ophthalmology*. 2006;113:1354–1362.
5. Bullimore MA, Brennan NA. Myopia control: why each diopter matters. *Optom Vis Sci*. 2019;96:463–465.
6. Verkicharla PK, Ohno-Matsui K, Saw SM. Current and predicted demographics of high myopia and an update of its associated pathological changes. *Ophthalmic Physiol Opt*. 2015;35:465–475.
7. Parolini B, Palmieri M, Finzi A, et al. The new myopic traction maculopathy staging system. *Eur J Ophthalmol*. 2021;31:1299–1312.
8. Cheong KX, Xu L, Ohno-Matsui K, Sabanayagam C, Saw SM, Hoang QV. An evidence-based review of the epidemiology of myopic traction maculopathy. *Surv Ophthalmol*. 2022;67:1603–1630.
9. Pan AP, Wan T, Zhu SQ, Dong L, Xue AQ. Clinical investigation of the posterior scleral contraction to treat macular traction maculopathy in highly myopic eyes. *Sci Rep*. 2017;7:43256.
10. Liu L, Rong H, Wu D, et al. Analysis of morphological and quantitative changes in pathological myopia and perioperative changes in posterior scleral reinforcement using three-dimensional magnet resonance imaging. *Front Bioeng Biotechnol*. 2023;11:1242440.
11. Zhang Z, Qi Y, Wei W, et al. Investigation of macular choroidal thickness and blood flow change by optical coherence tomography angiography after posterior scleral reinforcement. *Front Med (Lausanne)*. 2021;8:658259.
12. Wu H, Zhang G, Shen M, et al. Assessment of choroidal vascularity and choriocapillaris blood perfusion in anisomyopic adults by SS-OCT/OCTA. *Invest Ophthalmol Vis Sci*. 2021;62:8.
13. He Q, Wang X, Shi Q, Xie C, Xue A, Wei R. Posterior scleral reinforcement for the treatment of myopic traction maculopathy. *BMC Ophthalmol*. 2022;22:273.
14. Xue A, Zheng L, Tan G, et al. Genipin-crosslinked donor sclera for posterior scleral contraction/reinforcement to fight progressive myopia. *Invest Ophthalmol Vis Sci*. 2018;59:3564–3573.
15. Ye J, Pan AP, Zhu S, Zheng L, Lu F, Xue AQ. Posterior scleral contraction to treat myopic foveoschisis in highly myopic eyes. *Retina*. 2021;41:1047–1056.
16. Zhu S, Xue A, Li H, et al. Posterior scleral contraction to treat myopic traction maculopathy at different stages. *Am J Transl Res*. 2022;14:389–395.
17. Ohno-Matsui K, Akiba M, Modegi T, et al. Association between shape of sclera and myopic retinochoroidal lesions in patients with pathologic myopia. *Invest Ophthalmol Vis Sci*. 2012;53:6046–6061.
18. Shinohara K, Shimada N, Moriyama M, et al. Posterior staphylomas in pathologic myopia imaged by widefield optical coherence tomography. *Invest Ophthalmol Vis Sci*. 2017;58:3750–3758.
19. An G, Dai F, Wang R, et al. Association between the types of posterior staphyloma and their risk factors in pathological myopia. *Transl Vis Sci Technol*. 2021;10:5.
20. Lai TT, Huang CW, Yang CM. Postoperative large intraretinal cavity and schisis with paravascular inner break in high myopia. *Jpn J Ophthalmol*. 2023;67:66–73.
21. Ma IH, Hsieh YT, Yeh PT, Yang CH, Yang CM. Long-term results and risk factors influencing outcome of gas tamponade for myopic foveoschisis with foveal detachment. *Eye (Lond)*. 2020;34:392–399.
22. Jiang J, Yu X, He F, et al. Treatment of myopic foveoschisis with air versus perfluoropropane: a retrospective study. *Med Sci Monit*. 2017;23:3345–3352.
23. Toyama T, Roggia MF, Yamaguchi T, Noda Y, Ueta T. The extent of stretched lamellar cleavage and visual acuity in macular pseudoholes. *Br J Ophthalmol*. 2016;100:1227–1231.
24. Zhang XF, Qiao LY, Li XX, et al. A preliminary study on macular retinal and choroidal thickness and blood flow change after posterior scleral reinforcement by optical coherence tomography angiography. *Zhonghua Yan Ke Za Zhi*. 2017;53:39–45.
25. Agrawal R, Gupta P, Tan KA, Cheung CM, Wong TY, Cheng CY. Choroidal vascularity index as a measure of vascular status of the choroid: measurements in healthy eyes from a population-based study. *Sci Rep*. 2016;6:21090.
26. Agrawal R, Ding J, Sen P, et al. Exploring choroidal angioarchitecture in health and disease

using choroidal vascularity index. *Prog Retin Eye Res*. 2020;77:100829.
27. Breher K, Terry L, Bower T, Wahl S. Choroidal biomarkers: a repeatability and topographical comparison of choroidal thickness and choroidal vascularity index in healthy eyes. *Transl Vis Sci Technol*. 2020;9:8.
28. Rong H, Liu L, Liu Y, et al. Quantifying the morphology of eyeballs with posterior staphyloma with Zernike polynomials. *Front Bioeng Biotechnol*. 2023;11:1126543.
29. Wen B, Yang G, Cheng J, et al. Using high-resolution 3D magnetic resonance imaging to quantitatively analyze the shape of eyeballs with high myopia and provide assistance for posterior scleral reinforcement. *Ophthalmologica*. 2017;238:154–162.
30. Zou J, Tan W, Li F, et al. Outcomes of a new 3-D printing-assisted personalized macular buckle combined with para plana vitrectomy for myopic foveoschisis. *Acta Ophthalmol*. 2021;99:688–694.